HHS Public Access

Author manuscript

Nano Lett. Author manuscript; available in PMC 2016 October 02.

Published in final edited form as:

Nano Lett. 2016 May 11; 16(5): 3202–3209. doi:10.1021/acs.nanolett.6b00599.

Gd(III)-Dithiolane Gold Nanoparticles for T_1-Weighted Magnetic Resonance Imaging of the Pancreas

Robert J. Holbrook[†], **Nikhil Rammohan**[†], **Matthew W. Rotz**[†], **Keith W. MacRenaris**[†], **Adam T. Preslar**[†], and **Thomas J. Meade**[*,†]

[†]Department of Chemistry, Molecular Biosciences, Neurobiology, Radiology, and Center for Advanced Molecular Imaging, Northwestern University, Evanston, Illinois 60208, United States

Abstract

Pancreatic adenocarcinoma has a 5 year survival of approximately 3% and median survival of 6 months and is among the most dismal of prognoses in all of medicine. This poor prognosis is largely due to delayed diagnosis where patients remain asymptomatic until advanced disease is present. Therefore, techniques to allow early detection of pancreatic adenocarcinoma are desperately needed. Imaging of pancreatic tissue is notoriously difficult, and the development of new imaging techniques would impact our understanding of organ physiology and pathology with applications in disease diagnosis, staging, and longitudinal response to therapy in vivo. Magnetic resonance imaging (MRI) provides numerous advantages for these types of investigations; however, it is unable to delineate the pancreas due to low inherent contrast within this tissue type. To overcome this limitation, we have prepared a new Gd(III) contrast agent that accumulates in the pancreas and provides significant contrast enhancement by MR imaging. We describe the synthesis and characterization of a new dithiolane-Gd(III) complex and a straightforward and scalable approach for conjugation to a gold nanoparticle. We present data that show the nanoconjugates exhibit very high per particle values of r_1 relaxivity at both low and high magnetic field strengths due to the high Gd(III) payload. We provide evidence of pancreatic tissue labeling that includes MR images, post-mortem biodistribution analysis, and pancreatic tissue evaluation of particle localization. Significant contrast enhancement was observed allowing clear identification of the pancreas with contrast-to-noise ratios exceeding 35:1.

[*]**Corresponding Author**, tmeade@northwestern.edu. .

Supporting Information

The Supporting Information is available free of charge on the ACS Publications website at DOI: 10.1021/acs.nanolett.6b00599. (Figure S1) Synthesis of Lip-DO3A and Lip-DTPA; (Figure S2 and S3) proton and carbon-13 NMR spectra of Lip-NHS; (Figures S4 and S5) ESI-MS spectra of Lip-DO3A and Lip-DTPA; (Figure S6) HPLC chromatogram of pure Lip-DTPA; (Figure S7) MR images of additional mice; (Figure S8) Quantification of pancreas CNRs in controls versuss Lip-Gd@AuNPs. (PDF)

Author Contributions

R.J.H, M.W.R, K.W.M, and N.R designed experiments; R.J.H, M.W.R, K.W.M, A.T.P., and N.R.carried out experiments; R.J.H analyzed experimental results; R.J.H, M.W.R, N.R., and T.J.M. wrote the manuscript.

Notes

The authors declare no competing financial interest.

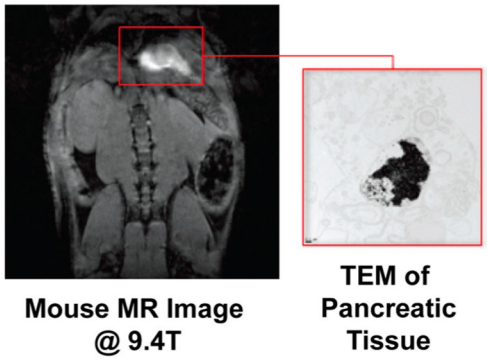

Keywords

Pancreas; magnetic resonance imaging; gold nanoparticles

Pancreatic cancer is a leading cause of cancer death worldwide and bears the poorest prognosis of any major malignancy.[1] With a 5 year survival of approximately 3% and median survival of 6 months, it has among the most dismal of all prognoses in medicine. While outcomes for other cancer types have improved steadily in the past few decades, results for pancreatic cancer have not changed significantly. The poor prognosis is largely due to delayed diagnosis where 80% of patients remain asymptomatic until affected by local or distant metastases. Furthermore, at this late stage, only 20% of patients can benefit from surgery and adjuvant chemotherapy, which extends 5 year survival to 20%.[2] The first-line imaging techniques used for diagnosis and preoperative staging of pancreatic cancer are abdominal ultrasound and computed tomography, but these modalities have diagnostic value at only an advanced disease stage.[3] The shortcomings of the currently available techniques for pancreatic cancer detection make it clear that new diagnostic approaches are needed.

MR imaging has emerged as an established technique for preclincal imaging and clinical diagnosis.[4–6] It provides tomographic information on live biological specimens with high spatiotemporal resolution and excellent soft tissue contrast without the use of radiotracers or ionizing radiation. As a result, long-term longitudinal studies are possible without harm to the specimen.[4–6] However, lack of intrinsic contrast can limit definitive detection of desired tissue. In these cases, contrast agents (CAs) are used to differentiate tissue types that would otherwise be indistinct. Paramagnetic chelates of Gd(III) are commonly used as CAs, as they shorten the longitudinal relaxation times (T_1) of proximal water protons in regions of CA accumulation and as a result generate positive image contrast.[5] The efficiency of a CA to reduce T_1 of surrounding water protons is determined by the CA's concentration and relaxivity, r_1 ($mM^{-1}\ s^{-1}$), as defined by eq 1.

$$\frac{1}{T_1}=\frac{1}{T_{1,\mathrm{Solvent}}}+r_1\,[Gd\,(III)] \quad (1)$$

Because of the dependency of T_1 on the concentration of Gd(III), CA accumulation strategies that target specific biological areas are being investigated.[7–9] Recently, CAs utilizing small molecule targeting or nanomaterial platforms have been shown to deliver Gd(III) to regions of interest, providing greater accumulation, and subsequent shorter T_1 for increased MR contrast enhancement.[10–13]

Specifically, Gd(III) labeled gold nanoparticles (AuNPs) are highly effective CAs for MR imaging.[14–20] To this end, our lab has developed Gd(III) enriched polyvalent DNA–gold nanoparticle conjugates (DNA–Gd@AuNP) for cell delivery and Gd(III) accumulation.[12,13] These conjugates have shown high biocompatibility, excellent stability, and high Gd(III) loading of polyvalent DNA AuNPs. However, in vivo targeting through systemic administration of polyvalent DNA AuNPs can be challenging due to their relatively fast clearance rates. Further functionalization of poly(ethylene gycol) (PEG) through thiol conjugation to the AuNP construct has been used to extend the circulation time and improve biological targeting. Previous studies by Mukherjee et al. have shown the surface charge of AuNPs using small molecule PEG surface ligands can fine-tune the circulation time and biodistribution through the systemic intravenous (iv) and intraperitoneal (ip) administration of AuNPs.[21] Interestingly, these AuNPs were observed to accumulate predominately in the pancreas of athymic nude mice through ip administration due to intraperitoneal circulation and altered lymphatic clearance.

Here, we describe the first Gd(III) based CAs for labeling and visualizing the pancreas using MRI. Through functionalization of spherical 17.2 nm AuNPs with small molecule Gd(III) CAs (Lip-Gd@AuNPs), we have developed a strategy for Gd(III) accumulation and image contrast enhancement in the pancreas by systemic ip administration. To investigate this Lip-Gd@AuNP system, two Gd(III) CAs, tetraazacyclododecanetriacetic acid (DO3A) and diethylenetriaminepentaacetic acid (DTPA), were modified with a terminal dithiolane ring through conjugation to lipoic acid. These two chelates (referred to as Lip-DO3A and Lip-DTPA) were subsequently conjugated to the AuNP surface using gold–thiol chemistry to form Lip-DO3A@AuNP and Lip-DTPA@AuNP, respectively (Scheme 1). ip administration of Lip-Gd@AuNPs to C57 black mice are shown to accumulate to the pancreas and provide significant enhancement of image contrast at 9.4 T (with contrast-to-noise ratios exceeding 35:1). This Lip-Gd@AuNP system provides a nanomaterial that utilizes the surface properties for high Gd(III) CA loading of AuNPs and localization to pancreatic tissue for MR imaging.

Results

Synthesis

An amine-functionalized DO3A-based Gd(III) complex containing a six carbon linker and a DTPA-based Gd(III) complex containing a four-carbon linker were synthesized according to previous reported procedures[22] and covalently attached to lipoic acid through peptide coupling to form Lip-DO3A and Lip-DTPA, respectively (see Supporting Information). Citrate-stabilized spherical AuNPs were fabricated using the Frens protocol according to previously published procedures.[23] The diameter of the particles was determined to be 17.2 ± 2.1 nm via analysis of images obtained by transmission electron microscopy (TEM) and

verified by dynamic light scattering (DLS), which indicated a hydrodynamic size of 20.2 ± 0.1 nm. Functionalization of the citrate-stabilized AuNPs with Lip-DO3A and Lip-DTPA were performed using 25 mL of 10 nM AuNPs with 0.01% Tween 20 (v/v). The complexes, Lip-DO3A and Lip-DTPA, were dissolved in 500 μL of methanol and 500 μL of Milli-Q water, added to the AuNP solution, and shaken overnight for the formation of Lip-DO3A@AuNP and Lip-DTPA@AuNP, respectively. Notably, Gd(III) conjugation to the AuNP surface is achieved without the addition of a reducing agent. Nanoconjugates were purified and concentrated by successive rounds of centrifugation.

Characterization of Gd(III) Loading

To quantify Gd(III) loading, inductively coupled plasma mass spectrometry (ICPMS) was used to determine the ratio of Gd(III) to Au. The Lip-DO3A@AuNP construct contained 2375 ± 81 Gd(III) complexes/AuNP, corresponding to a packing density of 2.54 ± 0.13 Gd(III) chelates/nm^2 of AuNP surface. The Lip-DTPA@AuNP contained 1477 ± 47 Gd(III) complexes/AuNP, corresponding to a packing density of 1.58 ± 0.09 Gd(III) chelates/nm^2 of AuNP surface. The negative charge of Lip-DTPA may decrease the packing density on the surface of the particle, relative to the neutrally charged Lip-DO3A. The loading of Lip-DO3A@AuNP and Lip-DTPA@AuNP represents greater than a 3- and 2-fold increase in Gd(III) payload and packing density, respectively, relative to previously reported DNA-Gd@AuNP (564 Gd(III)/AuNP and 0.8 Gd(III)/nm^2 of AuNP).[12] This phenomenon is attributed to the efficient packing of small molecular Gd(III) chelates relative to polyvalent DNA-Gd(III) conjugates on the surface of the AuNP.

Assessment of Relaxivity

To assess the performance of Lip-Gd@AuNPs, the r_1 was determined by taking the slope of the linear plot of T_1^{-1} versus Gd(III) concentration at low field (1.41 T) and high field (7 T) (Table 1). The Lip-DO3A@AuNP was observed to have an ionic r_1 of 14.6 ± 0.7 and 4.0 ± 0.1 mM^{-1} s^{-1} at 1.41 and 7 T, respectively. On the basis of particle loading of Lip-DO3A@AuNPs, this yields a per particle r_1 of 34 675 ± 2040 and 9500 ± 402 mM^{-1} s^{-1} at 1.41 and 7 T, respectively. The Lip-DTPA@AuNP was observed to have an ionic r_1 of 13.7 ± 0.8 and 4.7 ± 0.2 mM^{-1} s^{-1} at 1.41 and 7 T, respectively. On the basis of particle loading of Lip-DTPA@AuNPs, this yields a per particle r_1 of 20 235 ± 1346 and 6942 ± 369 mM^{-1} s^{-1} at 1.41 and 7 T, respectively. The ionic relaxivity of both DO3A@AuNPs and Lip-DTPA@AuNPs are comparable to previously reported DNA-Gd@AuNPs with an r_1 of 14.6 mM^{-1} s^{-1} at 1.41 T.[12] The ionic r_1 values of the Lip-Gd@AuNP system reflects an expected increase in relaxivity due to an increase in the rotational correlation time, τ_r, from conjugation to the AuNP surface by ultimately slowing the Gd(III) reorientation time.

Mouse MRI

In vivo imaging of animals incubated with Lip-Gd@AuNPs was conducted to measure enhanced MR image contrast in pancreatic tissue. In particular, pancreatic imaging in rodents can be challenging because the organ is not a well-defined solid retroperitoneal organ but rather a thin membrane spread throughout the upper abdomen and lying immediately adjacent to the gut.[24] Furthermore, the low intrinsic T_1-weighted contrast of the

pancreas, motion artifacts, and intestinal gas makes MR detection of the pancreas notoriously difficult. In an effort to evaluate the performance of Gd(III)@AuNPs for pancreatic imaging, animals were injected with 4.0 nmol/kg body weight of AuNPs through ip administration. For Lip-DO3A@AuNPs, this equates to 8.8 μmol/kg body weight of Gd(III). For Lip-DTPA@AuNPs, this equates to 5.5 μmol/kg body weight of Gd(III). Following ip injection and 24 h incubation, MR images were acquired of the peritoneal cavity at 9.4 T (n = 3 for Lip-DO3A@AuNP and Lip-DTPA@AuNP, respectively) using standard T_1-weighted FLASH scans. Significantly increased contrast enhancement was observed for mice treated with Lip-Gd@AuNPs, allowing obvious identification of the pancreas, with high contrast-to-noise ratios (CNRs) in all subjects (Figure 1). The muscle signal was subtracted from each pixel in the pancreas region of interest (ROI) and divided by the standard deviation of the noise to generate the CNR map. The resulting CNR maps were set to a threshold at a value of 35 and the number of pixels in the pancreas ROI of each mouse was counted (see Figures S7 and S8). The number of pixels with a CNR greater than 35 ranged from 343 to 805 for Lip-DO3A@AuNPs and from 178 to 364 for Lip-DTPA. Furthermore, the two control mice were observed to have 27 and 174 pixels with CNRs greater than 35. The marked increase in CNR of the T_1-weighted images of mice dosed with Lip-Gd@AuNPs indicates the localization of particles within the pancreas and subsequent contrast enhancement.

Biodistribution Analysis

To investigate the performance observed in MR imaging, biodistribution of Lip-Gd@AuNPs was conducted. Animals were sacrificed and organs were harvested for quantification of Gd(III) and Au using ICP-MS (n = 5 for Lip-DO3A@AuNP and Lip-DTPA@AuNP, respectively; Figure 2). Significant accumulation in the liver and spleen was observed (~700 and ~400 μg of Au per gram of tissue, respectively, for both Lip-DO3A@AuNPs and Lip-DTPA@AuNPs). The high levels of AuNPs found in the liver and spleen suggest that the reticuloendothelial system (RES) is the dominant mode of clearance for these particles.[25,26] However, despite this high accumulation, no significant MR contrast enhancement is observed in these organs when compared to the pancreas. This phenomenon may be attributed to organ density and differences in contrast agent diffusion rates within the tissues.[27] Importantly, significant localization to the pancreas was observed (~550 μg of Au per gram of tissue for both Lip-DO3A@AuNPs and Lip-Gd@AuNPs). Indeed, the levels of Gd(III) relative to Au in all tissues reflect the Gd(III) loading observed for Lip-DO3A@AuNPs and Lip-DTPA@ AuNPs and not the differences in charge of the two chelates. In general, the biodistribution of Lip-Gd@AuNPs through ip administration reflects previously reported behavior of small molecule, PEGylated AuNPs.[21,28,29] These results validate our approach toward accumulation to the pancreas through AuNP surface modification with hydrophilic, small molecule Gd(III) CAs.

In an effort to validate the accumulation of Lip-Gd@AuNPs to the pancreas, TEM and histology of the pancreas were performed following 24 h incubation with Lip-DO3A@AuNPs and Lip-DTPA@AuNPs, respectively. Immediately following harvesting of the pancreas, the tissue was divided in two and fixed in formalin. The tissue was separately prepared for sectioning for TEM and histology. TEM images of pancreatic tissue slices

revealed the presence of AuNPs in mice incubated with both Lip-Gd@AuNP constructs (Figure 2). Significant presence of particles was observed to be encapsulated in large particle aggregates in lysosomes (~1 μm) of macrophages and located in the interstitial spaces between acinar cells of the pancreatic tissue. The identification of the acinar cells was based on the presence of extensive endoplasmic reticulum (ER) organelles because they are indicative of this particular pancreatic cell type.

Further confirmation of pancreatic tissue labeling by Lip-Gd@AuNPs was obtained through histological analysis. The presence of AuNP aggregates is observed in hematoxylin and eosin stained pancreatic tissue sections for animals incubated with Lip-DO3A@AuNPs and Lip-DTPA@AuNPs, respectively (Figure 2). No structural and morphological abnormalities were noted in either of the two pancreases. However, slight inflammation was noted in the adjacent fatty tissues. Under high-power magnification (100×), black AuNP aggregates are diffusely distributed in the surrounding fatty tissue of the pancreas. The inflammatory cells include lymphocytes and histiocytes and nanoparticle-laden phagocytes. Furthermore, the tissue contained nanoparticle aggregates directly in the pancreatic tissue among acinar cells. While we have not established a mechanism of organ localization, we hypothesize that Lip-Gd@AuNPs (when delivered by ip administration) can elicit an immune response that drives accumulation to the pancreas through sequestration by macrophages.[21,30]

Discussion

The advantages of Lip-Gd@AuNP described here provide the first methods for using T_1-weighted MRI CAs for imaging the pancreas. The functionalization of AuNPs and increased surface loading of Gd(III) were demonstrated by ICP-MS during the synthesis and development of the Lip-Gd@AuNP system. Biodistribution experiments showed that both Lip-DO3A@AuNPs and Lip-DTPA@AuNPs accumulate to the pancreas. Furthermore, by TEM and histological analysis we found that significant nanoparticle labeling occurs through uptake by macrophages within the pancreatic tissue. As a result, unprecedented MR image contrast enhancement of the pancreas was observed.

Lip-Gd@AuNPs are the first MRI contrast agents of any type, either paramagnetic or superparamagnetic, to effectively image the pancreas. Targeting to the pancreas is a significant challenge because the organ is hypovascular and surrounded by abundant fibrous stroma and fatty tissue.[31,32] Other CA formulations utilizing iron oxide,[33,34] manganese,[35,36] or gadolinium[37,38] for MR imaging of the pancreas have been unconvincing. In this context, the efficacy of Lip-Gd@AuNPs for pancreatic MRI is compelling, but several features of this platform need further exploration.

First, the lack of appreciable contrast in the liver and spleen is surprising, given the nearly equal Gd(III) content in those tissues compared to the pancreas (Figure 2). This may be due to differences in tissue density and contrast agent diffusion within tissue between the three organs. The mouse pancreas is a thin, membranous organ[24] where localized particle accumulation was observed by TEM and histology and resulted in high image contrast in T_1-weighted imaging. However, the mouse liver and spleen are dense organs, where diffusely distributed Gd(III) may not result in similar image contrast. Further study is

required to understand and correlate particle diffusion and behavior within different tissue types and the image contrast produced in T_1-weighted imaging.

While the accumulation of Lip-Gd@AuNPs in the liver and spleen can be explained by their function as clearance organs, the mechanism by which Lip-Gd@AuNPs accumulate specifically in the pancreas is currently unknown. Studies are underway to explore which features of the nanoparticle construct, that is, size, shape, charge, or gadolinium–gold surface chemistry, contribute toward pancreatic localization. On the basis of significant accumulation of Lip-Gd@AuNPs in macrophages in pancreatic tissue, we hypothesize that targeting to the pancreas is achieved via macrophage uptake by tissue-resident and peritoneal macrophages homing to the pancreas. Accordingly, the recruitment, phenotype, and inflammatory response of macrophages during administration and action of Lip-Gd@AuNPs should be evaluated.

In conclusion, Lip-Gd@AuNPs provide a robust platform for the development of pancreas-specific MR imaging agents, which may prove invaluable in the diagnosis and treatment of pancreatic disease.

Materials and Methods

General Synthesis Methods

Unless noted, solvents and reagents were purchased from Sigma-Aldrich Chemical Co. (St. Louis, MO) and used without further purification. All reactions were performed under nitrogen atmosphere unless otherwise stated. Solvents including tetrahydrofuran (THF), dimethylformamide (DMF), dimethyl sulfoxide (DMSO), and methanol (MeOH) were dried and purified using a Glass Contour Solvent system. Deionized water was obtained from a Millipore Q-Gard System equipped with a quantum Ex cartridge (Billerica, MA). Standard grade 60 Å 230–400 mesh silica gel (Machery-Nagel) was used for flash column chromatography.

Proton (^{1}H) and carbon (^{13}C) NMR spectra were obtained on a 500 MHz Avance III NMR Spectrometer or a Bruker 600 MHz Avance III NMR spectrometer with deuterated solvent as noted. Electrospray ionization mass spectrometry (ESI-MS) spectra were taken on a Bruker AmaZon SL Ion Trap instrument. Reverse phase analytical HPLC-MS was performed on a Varian Prostar 500 system with a Waters 4.6 × 250 mm 5 μM Atlantis C18 column. This system was equipped with a Varian 380 LC ELSD system, a Varian 363 nm fluorescence detector, and a Varian 335 nm UV–vis detector. After method development, preparative runs were performed using a Waters 19 × 250 mm Atlantis C18 column. The mobile phases consisted of Millpore water and HPLC-grade acetonitrile.

Quantification of gadolinium and gold was performed using inductively coupled plasma mass spectrometry (ICP-MS). For sample preparation, chemical analyses were performed by digestion of particle solutions in 1:1 concentrated nitric acid (>69%) and concentrated hydrochloric acid (37%) and placed at 75 °C for 4 h for digestion. Biodistribution analyses required using the same 1:1 acid composition, and subsequent microwave heating for complete organ digestion (Milestone Ethos EZ, Stamford, CT). The digestate of organ

samples were then used for preparation of ICP solutions by the same method as chemical analyses. Specifically, ultrapure H_2O (18.2 MΩ·cm) and multielement internal standard containing Bi, Ho, In,^{6}Li, Sc, Tb, and Y (CLISS-1, Spex Certiprep, Metuchen, NJ, U.S.A.) were added to digestate to produce a final solutions of 2% nitric acid (v/v), 2% HCl (v/v), and 5.0 ng/mL internal standard in a total sample volume of 10 mL. Individual Au and Gd elemental standards were prepared at 0, 0.78125, 1.5625, 3.125, 6.25, 12.5, 25.0, 50.0, 100, and 200 ng/mL concentrations with 2% nitric acid (v/v), 2% HCl (v/v) and 5.0 ng/mL internal standards up to a total sample volume of 5 mL.

ICP-MS was performed on a computer-controlled (QTEGRA software) Thermo icapQc ICP-MS (Thermo Fisher Scientific, Waltham, MA, U.S.A.) operating in standard mode and equipped with a CETAC 260 autosampler (Omaha, NE, U.S.A.). Each sample was acquired using 1 survey run (10 sweeps) and 3 main (peak jumping) runs (100 sweeps). The isotopes selected were ^{197}Au, ^{156,157}Gd, ^{115}In, ^{165}Ho, and ^{209}Bi (as internal standards for data interpolation and machine stability). Instrument performance was optimized daily through autotuning followed by verification via a performance report (passing manufacturer specifications).

Synthesis of Lipoic Acid N-Hydroxysuccinimidyl Ester (Lip-NHS)

To a 100 mL round-bottom flask containing a magnetic stir bar and (±)-lipoic acid (0.500 g, 2.4 mmol) and *N*-hydroxysuccinimide (0.418 g, 3.6 mmol) was added 20 mL of chloroform. The mixture was stirred at room temperature until dissolution of the NHS at which time was added *N,N*′-diisopropylcarbodiimmide (0.563 mL, 3.6 mmol) dropwise at room temperature. Complete formation of the coupled NHS ester was assessed by the appearance of product by TLC (R_f = 0.4) in diethyl ether and was visualized by CAM stain. Purification of the product was achieved by silica gel chromatography in 100% diethyl ether resulting in an 80% yield. Proton and carbon NMR spectra are shown in Figures S2 and S3. ^{1}H NMR (500 MHz, Chloroform-*d*) *δ*: 3.64–3.53 (m, 1H), 3.24–3.07 (m, 2H), 2.84 (s, 4H), 2.63 (t, *J* = 7.3 Hz, 2H), 2.47 (q, *J* = 12.3, 6.6 Hz, 1H), 1.92 (q, *J* = 13.5, 6.9 Hz, 1H), 1.85–1.43 (m, 7H). ^{13}C NMR (126 MHz, $CDCl_3$) *δ*: 169.10, 168.40, 56.09, 40.15, 38.52, 34.42, 30.79, 28.32, 25.59, 24.37. ESI-MS (*m/z*): observed, 617.1; calculated, 617.1 $[M]^-$

Synthesis of Lip-DO3A

To a 10 mL round-bottom flask containing a magnetic stir bar was added previously reported Gd-DO3A-C6 amine (0.100 g, 0.17 mmol) in 1 mL of carbonate buffer pH 9.2. In a separate vial was added Lip-NHS (0.08 g, 0.20 mmol) and 2 mL DMSO. Upon complete dissolution of lipoic acid NHS-ester, the solution was added to the stirring solution of Gd-DO3A-C6 amine at room temperature and left to stir for 12 h. Purification of the final product was achieved by semipreparative HPLC. The crude mixture was injected directly, eluting via the use of the following method, where the mobile phase consisted of Millipore water and HPLC grade acetonitrile (ACN); initial conditions of 0% ACN were held constant for 5 min, then ramped to 32% ACN between 5–17 min, followed by a gradual ramp to 40% ACN at 31 min. The product peak eluted between 23 and 26 min, as monitored by UV absorption at 210 nm. The product was collected and lyophilized to a fluffy pale yellow solid. ESI-MS

spectrum is shown in Figure S4. ESI-MS (*m/z*): observed, 811.0; calculated, 811.1 [M + Na]$^+$.

Synthesis of Lip-DTPA

Lip-DTPA was synthesized by an analogous procedure to Lip-DO3A. Specifically, a 10 mL round-bottom flask was charged with a magnetic stir bar and previously reported Gd-DTPA-C4 amine (0.100 g, 0.16 mmol) in 1 mL of carbonate buffer pH 9.2. In a separate vial was added lipoic acid NHS-ester (0.08 g, 0.20 mmol) and 2 mL of DMSO. Upon complete dissolution of Lip-NHS, the solution was added to the stirring solution of Gd-DTPA-C4 amine at room temperature and left to stir for 12 h. Reaction completeness was monitored by ESI-MS for the disappearance of starting material. Purification of final product was achieved by semipreparative HPLC. The crude mixture was injected directly, eluting via the use of the following method, where the mobile phase consisted of Millipore water and HPLC grade acetonitrile (ACN); initial conditions of 0% ACN were held constant for 5 min, then ramped to 5% ACN between 5–10 min, and held constant at 5% ACN until 20 min. Acetonitrile was then ramped to 100% through 25 min and held constant at 100% ACN until 30 min. The product peak eluted between 26.0 and 26.9 min, as monitored by UV absorption at 210 nm (chromatogram of pure product shown in Figure S6). ESI-MS spectrum is shown in Figure S5. ESI-MS (*m/z*): observed, 805.02; calculated, 805.2 [M$^-$]

Synthesis of Citrate-Stabilized AuNP

Gold nanoparticles were synthesized by citrate reduction of gold chloride. Specifically, $HAuCl_4$ trihydrate (0.197 g) was dissolved in 498 mL of Millipore water in an acid washed two-necked round-bottom flask and brought to reflux. To the boiling mixture was added trisodium citrate (0.509 g) in 2 mL of water, and the solution was left to boil for 30 min. Particles were filtered using a 200 nm filter, the plasmon resonance wavelength was observed by UV/vis spectroscopy, and size was confirmed by DLS and TEM. Final particle concentration was determined using ICP-MS.

Particle size was determined by examination of over 100 particles using ImageJ, and volume and total gold content approximations were made by using the geometric formula for the volume of a sphere and the density of bulk gold (59.01 Au/nm^3).

Synthesis of Lip-Gd@AuNPs

Functionalization of the citrate stabilized AuNPs with Lip-DO3A or Lip-DTPA were performed using 25 mL of 10 nM AuNPs with 0.01% Tween 20 (v/v). The complexes, Lip-DO3A and Lip-DTPA, were dissolved in 500 μL of methanol and 500 μL of Millipore water, added to the AuNP solution, and shaken overnight for the formation of Lip-DO3A@AuNP and Lip-DTPA@AuNP, respectively. Notably, functionalization of the AuNP surface was achieved without the addition of a reducing agent. The functionalized AuNPs were purified and concentrated using ultracentrifugation. Five rounds of centrifugation at 21.1×*g* (20 min, 7 °C) were performed to sediment the particles. Following each round of centrifugation, the top solution was subsequently decanted, and the particles were resuspended in Dulbecco's phosphate buffered saline (DPBS) with 0.01% Tween 20. The particles were concentrated

down to 250 nM AuNPs as a 1 mL stock solution in DPBS 0.01% Tween 20. When not in use, particles were stored at 4 °C.

Low-Field Relaxivity (1.41 T)

A stock solution of Lip-Gd@AuNP was made (700 uL). This stock was serially diluted four times for a total of five solutions. Solutions were heated to 37 °C and 150 uL of each concentration was placed into a Bruker minispec mq60 NMR spectrometer (60 MHz) for measurement of T_1 relaxation time. Data were collected using an inversion recovery pulse sequence using 4 averages, a 15 s repetition time, and 10 data points. The remaining volumes of each solution were utilized for ICP-MS analysis of [Gd(III)]. The inverse of the longitudinal relaxation time ($1/T_1$, s^{-1}) was plotted versus the Gd(III) concentration (mM). The slope that was generated by the plotting of this data was defined as the relaxivity of the agent ($mM^{-1}\ s^{-1}$).

High-Field Relaxivity (7 T)

MR imaging and T_1 measurements were performed on a Bruker Pharmscan 7 T imaging spectrometer fitted with shielded gradient coils at 25 °C. Samples were prepared by serial dilution and confirmation of concentration by ICP-MS for [Gd(III)]. Solutions were imaged in glass capillary tubes of approximate diameter = 1 mm.

Spin–lattice relaxation times (T_1) were measured using a rapid-acquisition rapid-echo (RARE-VTR) T_1-map pulse sequence with static TE (11 ms) and variable TR (150, 250, 500, 750, 1000, 2000, 4000, 6000, 8000, and 10 000 ms) values. Imaging parameters were as follows: field of view = 25 × 25 mm^2, matrix size (MTX) = 256 × 256, number of axial slices = 4, slice thickness (SI) = 1.0 mm, and averages = 3 (total scan time = 2 h 36 min). T_1 analysis was carried out using the image sequence analysis tool in Paravision 5.0 software (Bruker, Billerica, MA, U.S.A.) with monoexponential curve-fitting of image intensities of selected regions of interest (ROIs) for each axial slice.

Animal Studies

Male C-57 black mice (wild type) were acquired from Charles River (Wilminton, MA) and were housed under pathogen free conditions. All animal studies were conducted at Northwestern University in accordance with the National Institutes of Health Guide for the Care and Use of Laboratory Animals and established institutional animal use and care protocols.

MR Imaging

In vivo MR images ($n = 3$) were acquired 24 h post injection of Lip-Gd@AuNPs on a 9.4T Bruker Biospec (Bruker Biospin, Billerica, MA, U.S.A.) using a 38 mm quadrature mouse body volume coil. For anatomical reference, T_2 weighted accelerated spin echo (TurboRARE) images were acquired with TR/TE = 570 ms/24 ms, RARE factor 8, field of view 4 cm × 4 cm, matrix 256 × 256, 1 mm slice thickness, 7 slices, 0.3 mm slice gap, and 9 averages. To measure contrast enhancement, T_1 weighted gradient echo FLASH images were acquired with TR/TE/α = 100 ms/2.2 ms/45° and 2 averages. Slice geometry was identical to the T_2 weighted images except for a matrix of 192 × 192. During imaging, mice

were held under 1–2% inhaled isoflurane anesthesia and respiration was monitored using an SA Instruments MR compatible monitoring system (SA Instruments, Stonybrook, NY, U.S.A.). Images were processed using JIM 6 software (Xinapse Systems, Essex, United Kingdom). Contrast-to-noise ratio (CNR) maps were measured by placing a signal region of interest in leg skeletal muscle and the bladder, and a noise region in the corner of the image, subtracting muscle signal from each pixel in the image, and dividing by the standard deviation of the noise. For visualization, CNR maps were set to a threshold at a value of 35, a color lookup table was applied, and the map was overlaid on the T_2 weighted anatomical reference image.

Supplementary Material

Refer to Web version on PubMed Central for supplementary material.

ACKNOWLEDGMENTS

This work was supported by the National Institutes of Health's Centers of Cancer Nanotechnology Excellence initiative of the National Cancer Institute under Award U54CA151880 and the Rosenberg Cancer Foundation. Metal analysis was performed at the Northwestern University Quantitative Bioelemental Imagining Center generously supported by NASA Ames Research Center Grant NNA04CC36G. Imaging work was performed at the Northwestern University (NU) Center for Advanced Molecular Imaging (CAMI) with the help of Dr. Chad Haney and Dr. Alex Waters. Histological analysis was performed at the NU Mouse Histology and Phenotyping Laboratory (MHPL) with the help of Dr. Lin Li. Both CAMI and MHPL are generously supported by NCI CCSG P30 CA060553 awarded to the Robert H. Lurie Comprehensive Cancer Center. TEM imaging work was performed at the NU Biological Imaging Facility generously supported by the NU Office for Research with the help of Ms. Charlene Wilke.

REFERENCES

(1). Klein AP. Identifying people at a high risk of developing pancreatic cancer. Nat. Rev. Cancer. 2012; 13:66–74. [PubMed: 23222481]

(2). Abbruzzese J. The challenge of pancreatic cancer. Int. J. Gastrointest. Cancer. 2003; 33:1–2. [PubMed: 12909733]

(3). Hidalgo M, Cascinu S, Kleeff J, Labianca R, Löhr JM, Neoptolemos J, Real FX, Van Laethem J-L, Heinemann V. Addressing the challenges of pancreatic cancer: Future directions for improving outcomes. Pancreatology. 2015; 15:8–18. [PubMed: 25547205]

(4). Dempsey MF, Condon B, Hadley DM. MRI safety review. Seminars in Ultrasound, CT and MRI. 2002; 23:392–401.

(5). Shellock FG, Spinazzi A. MRI Safety Update 2008: Part 1, MRI Contrast Agents and Nephrogenic Systemic Fibrosis. AJR, Am. J. Roentgenol. 2008; 191:1129–1139. [PubMed: 18806155]

(6). Willinek WA, Schild HH. Clinical advantages of 3.0 T MRI over 1.5 T. Eur. J. Radiol. 2008; 65:2–14. [PubMed: 18162354]

(7). Harrison VSR, Carney CE, MacRenaris KW, Waters EA, Meade TJ. Multimeric Near IR–MR Contrast Agent for Multimodal In Vivo Imaging. J. Am. Chem. Soc. 2015; 137:9108. [PubMed: 26083313]

(8). Strauch RC, Mastarone DJ, Sukerkar PA, Song Y, Ipsaro JJ, Meade TJ. Reporter Protein-Targeted Probes for Magnetic Resonance Imaging. J. Am. Chem. Soc. 2011; 133:16346–16349. [PubMed: 21942425]

(9). Sukerkar PA, MacRenaris KW, Meade TJ, Burdette JE. A Steroid-Conjugated Magnetic Resonance Probe Enhances Contrast in Progesterone Receptor Expressing Organs and Tumors in Vivo. Mol. Pharmaceutics. 2011; 8:1390–1400.

(10). Hung AH, Holbrook RJ, Rotz MW, Glasscock CJ, Mansukhani ND, MacRenaris KW, Manus LM, Duch MC, Dam KT, Hersam MC, Meade TJ. Graphene Oxide Enhances Cellular Delivery

of Hydrophilic Small Molecules by Co-incubation. ACS Nano. 2014; 8:10168–10177. [PubMed: 25226566]

(11). Jensen SA, Day ES, Ko CH, Hurley LA, Luciano JP, Kouri FM, Merkel TJ, Luthi AJ, Patel PC, Cutler JI, Daniel WL, Scott AW, Rotz MW, Meade TJ, Giljohann DA, Mirkin CA, Stegh AH. Spherical Nucleic Acid Nanoparticle Conjugates as an RNAi-Based Therapy for Glioblastoma. Sci. Transl. Med. 2013; 5:209ra152.

(12). Rotz MW, Culver KSB, Parigi G, MacRenaris KW, Luchinat C, Odom TW, Meade TJ. High Relaxivity Gd(III)–DNA Gold Nanostars: Investigation of Shape Effects on Proton Relaxation. ACS Nano. 2015; 9:3385–3396. [PubMed: 25723190]

(13). Song Y, Xu X, MacRenaris KW, Zhang X-Q, Mirkin CA, Meade TJ. Multimodal Gadolinium-Enriched DNA–Gold Nanoparticle Conjugates for Cellular Imaging. Angew. Chem., Int. Ed. 2009; 48:9143–9147.

(14). Alric C, Taleb J, Duc GL, Mandon C, Billotey C, Meur-Herland AL, Brochard T, Vocanson F, Janier M, Perriat P, Roux S, Tillement O. Gadolinium Chelate Coated Gold Nano-particles As Contrast Agents for Both X-ray Computed Tomography and Magnetic Resonance Imaging. J. Am. Chem. Soc. 2008; 130:5908–5915. [PubMed: 18407638]

(15). Park J-A, Reddy PAN, Kim H-K, Kim I-S, Kim G-C, Chang Y, Kim T-J. Gold nanoparticles functionalised by Gd-complex of DTPA-bis(amide) conjugate of glutathione as an MRI contrast agent. Bioorg. Med. Chem. Lett. 2008; 18:6135–6137. [PubMed: 18938074]

(16). Sung S, Holmes H, Wainwright L, Toscani A, Stasiuk GJ, White AJP, Bell JD, Wilton-Ely JDET. Multimetallic Complexes and Functionalized Gold Nanoparticles Based on a Combination of d- and f-Elements. Inorg. Chem. 2014; 53:1989–2005. [PubMed: 24495254]

(17). Irure A, Marradi M, Arnaiz B, Genicio N, Padro D, Penades S. Sugar/gadolinium-loaded gold nanoparticles for labelling and imaging cells by magnetic resonance imaging. Biomater. Sci. 2013; 1:658–668.

(18). Ferreira MF, Goncalves J, Mousavi B, Prata MIM, Rodrigues SPJ, Calle D, Lopez-Larrubia P, Cerdan S, Rodrigues TB, Ferreira PM, Helm L, Martins JA, Geraldes CFGC. Gold nanoparticles functionalised with fast water exchanging Gd3+ chelates: linker effects on the relaxivity. Dalton Transactions. 2015; 44:4016–4031. [PubMed: 25611006]

(19). Lewis DJ, Pikramenou Z. Lanthanide-coated gold nanoparticles for biomedical applications. Coord. Chem. Rev. 2014; 273–274:213–225.

(20). Zeng Y, Zhang D, Wu M, Liu Y, Zhang X, Li L, Li Z, Han X, Wei X, Liu X. Lipid-AuNPs@PDA Nanohybrid for MRI/CT Imaging and Photothermal Therapy of Hepatocellular Carcinoma. ACS Appl. Mater. Interfaces. 2014; 6:14266–14277. [PubMed: 25090604]

(21). Arvizo RR, Miranda OR, Moyano DF, Walden CA, Giri K, Bhattacharya R, Robertson JD, Rotello VM, Reid JM, Mukherjee P. Modulating Pharmacokinetics, Tumor Uptake and Biodistribution by Engineered Nanoparticles. PLoS One. 2011; 6:e24374. [PubMed: 21931696]

(22). Hung AH, Duch MC, Parigi G, Rotz MW, Manus LM, Mastarone DJ, Dam KT, Gits CC, MacRenaris KW, Luchinat C, Hersam MC, Meade TJ. Mechanisms of Gadographene-Mediated Proton Spin Relaxation. J. Phys. Chem. C. 2013; 117:16263–16273.

(23). Burda C, Chen X, Narayanan R, El-Sayed MA. Chemistry and Properties of Nanocrystals of Different Shapes. Chem. Rev. 2005; 105:1025–1102. [PubMed: 15826010]

(24). Grimm J, Potthast A, Wunder A, Moore A. Magnetic resonance imaging of the pancreas and pancreatic tumors in a mouse orthotopic model of human cancer. Int. J. Cancer. 2003; 106:806–811. [PubMed: 12866043]

(25). Lasagna-Reeves C, Gonzalez-Romero D, Barria MA, Olmedo I, Clos A, Sadagopa Ramanujam VM, Urayama A, Vergara L, Kogan MJ, Soto C. Bioaccumulation and toxicity of gold nanoparticles after repeated administration in mice. Biochem. Biophys. Res. Commun. 2010; 393:649–655. [PubMed: 20153731]

(26). Sadauskas E, Wallin H, Stoltenberg M, Vogel U, Doering P, Larsen A, Danscher G. Kupffer cells are central in the removal of nanoparticles from the organism. Part. Fibre Toxicol. 2007; 4:10. [PubMed: 17949501]

(27). Koh D-M, Collins DJ. Diffusion-Weighted MRI in the Body: Applications and Challenges in Oncology. AJR, Am. J. Roentgenol. 2007; 188:1622–1635. [PubMed: 17515386]

(28). Patra CR, Bhattacharya R, Mukhopadhyay D, Mukherjee P. Fabrication of gold nanoparticles for targeted therapy in pancreatic cancer. Adv. Drug Delivery Rev. 2010; 62:346–61.

(29). Patra CR, Bhattacharya R, Wang E, Katarya A, Lau JS, Dutta S, Muders M, Wang S, Buhrow SA, Safgren SL, Yaszemski MJ, Reid JM, Ames MM, Mukherjee P, Mukhopadhyay D. Targeted delivery of gemcitabine to pancreatic adenocarcinoma using cetuximab as a targeting agent. Cancer Res. 2008; 68:1970–8. [PubMed: 18339879]

(30). Bellingan GJ, Xu P, Cooksley H, Cauldwell H, Shock A, Bottoms S, Haslett C, Mutsaers SE, Laurent GJ. Adhesion Molecule–dependent Mechanisms Regulate the Rate of Macrophage Clearance During the Resolution of Peritoneal Inflammation. J. Exp. Med. 2002; 196:1515–1521. [PubMed: 12461086]

(31). Miller FH, Rini NJ, Keppke AL. MRI of adenocarcinoma of the pancreas. AJR, Am. J. Roentgenol. 2006; 187:W365–74. [PubMed: 16985107]

(32). Tummala P, Junaidi O, Agarwal B. Imaging of pancreatic cancer: An overview. J. Gastrointest. Oncol. 2011; 2:168–74. [PubMed: 22811847]

(33). Lee GY, Qian WP, Wang L, Wang YA, Staley CA, Satpathy M, Nie S, Mao H, Yang L. Theranostic nanoparticles with controlled release of gemcitabine for targeted therapy and MRI of pancreatic cancer. ACS Nano. 2013; 7:2078–89. [PubMed: 23402593]

(34). Torres GM, Erquiaga E, Ros PR, Burton SS, Barreda R, Langmo LS, Kennedy SJ. Preliminary results of MR imaging with superparamagnetic iron oxide in pancreatic and retroperitoneal disorders. Radiographics: a review publication of the Radiological Society of North America, Inc. 1991; 11:785–91.

(35). Botsikas D, Terraz S, Vinet L, Lamprianou S, Becker CD, Bosco D, Meda P, Montet X. Pancreatic magnetic resonance imaging after manganese injection distinguishes type 2 diabetic and normoglycemic patients. Islets. 2012; 4:243–8. [PubMed: 22722479]

(36). Diehl SJ, Lehmann KJ, Gaa J, McGill S, Hoffmann V, Georgi M. MR imaging of pancreatic lesions. Comparison of manganese-DPDP and gadolinium chelate. Invest. Radiol. 1999; 34:589–95. [PubMed: 10485075]

(37). Schima W. MRI of the pancreas: tumours and tumour-simulating processes. Cancer Imaging. 2006; 6:199–203. [PubMed: 17208676]

(38). Birchard KR, Semelka RC, Hyslop WB, Brown A, Armao D, Firat Z, Vaidean G. Suspected pancreatic cancer: evaluation by dynamic gadolinium-enhanced 3D gradient-echo MRI. AJR, Am. J. Roentgenol. 2005; 185:700–3. [PubMed: 16120921]

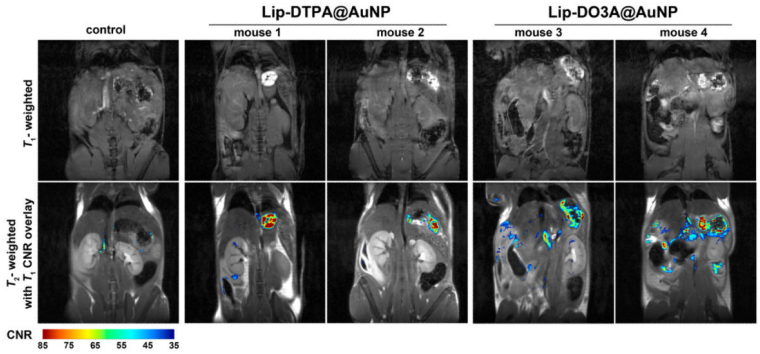

Figure 1.

T_1-weighted FLASH images were obtained at 9.4 T to assess contrast of Lip-DTPA@AuNPs and Lip-DO3A@AuNPs (n = 3; two images are displayed; see Figure S7). Contrast-to-noise ratio (CNR) relative to muscle, computed from T_1-weighted FLASH images, were overlaid on TurboRARE T_2-weighted anatomical images at 9.4 T after administration of Lip-DTPA@AuNPs, Lip-DO3A@AuNPs, and no agents (control) following 24 h incubation. Upon administration of both Lip-Gd@AuNP constructs, significant contrast enhancement is observed in the region of the pancreas.

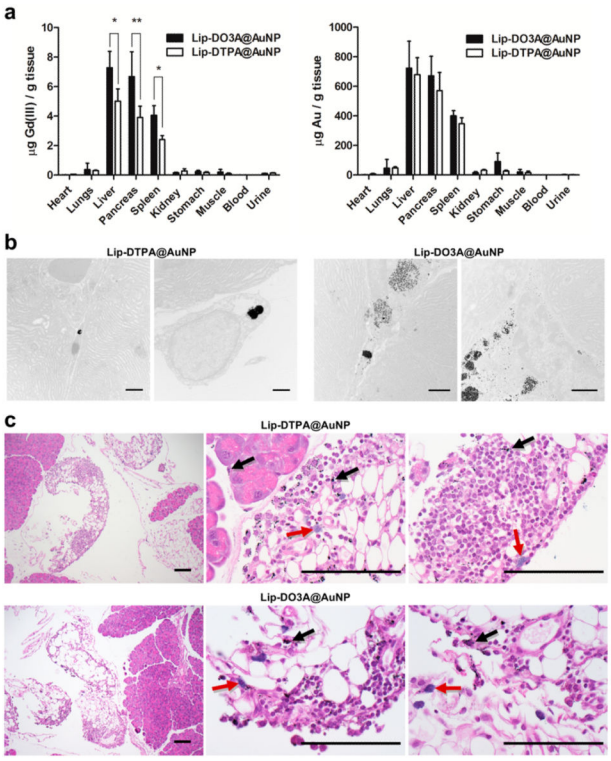

Figure 2.

(a) Biodistribution of Lip-DTPA@AuNPs and Lip-DO3A@AuNPs in C-57 mice. Following ip administration and 24 h incubation, organs were harvested and metal analysis was conducted via ICP-MS to determine the amount of Gd(III) and Au per gram of organ. Lip-Gd@AuNPs accumulate in the clearance organs, liver and spleen, and accumulates in the pancreas. Similar amounts of Au per gram of organ were observed for both Lip-DO3A@AuNP and Lip-DTPA@AuNP. However, Lip-DO3A@AuNP was observed to have a greater amount of Gd(III) per gram of organ, reflecting the higher Gd(III) loading onto the particle. Two-tailed t test: * $P < 0.01$, ** $P < 0.05$. (b) TEM images of pancreatic tissue from mice treated with Lip-DTPA@AuNPs and Lip-DO3A@AuNPs. Particles are present (as black spheres) in a lysosome as particle aggregates (<1 μm) in the macrophage. The labeled cell is present in the interstitial spaces of acrine cells as identified by the extensive ER organelles (scale bars are 1 μm). (c) Histology reveals mild inflammatory foreign material reaction in the adjacent tissue of the pancreas. The low-magnification images (10×) show Lip-DTPA@AuNPs and Lip-DO3A@AuNPs labeled pancreatic tissue and the adjacent fatty tissues. No structural or morphological abnormalities were noted in either of the two pancreases. Under the high-power magnification (100×), black nanoparticles are diffusely distributed in the fatty and pancreatic tissue (black arrows) of both pancreas slices. The inflammatory cells include lymphocytes and histocytes, some with phagocytic nanoparticles (red arrows) (scale bars are 100 μm).

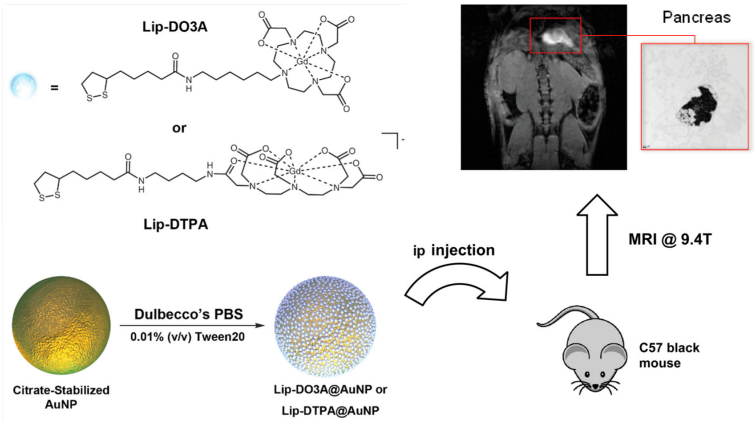

Scheme 1. Gd(III) Chelates (Lip-DO3A and Lip-DTPA) Were Conjugated to the Surface of AuNPs to Create Lip-DO3A@AuNP and Lip-DTPA@AuNP (for Synthesis Details, See Figure S1)[a]

[a]These constructs were injected into the ip cavity of C57 black wild-type mice. After 24 h, T_1-weighted MR images of the peritoneal cavity were acquired and revealed remarkable accumulation in the pancreas providing significant image contrast. TEM of fixed pancreatic tissue shows nanoparticle uptake in pancreatic cells (inset).

Table 1

Relaxivities of Lip-DO3A@AuNPs and Lip-DTPA@AuNPs at 1.41 and 7 T[a]

	$r_{1,ionic}$ (mM^{-1} s^{-1}) at 1.41 T	$r_{1,paritcle}$ (mM^{-1} s^{-1}) at 1.41 T	$r_{1,ionic}$ (mM^{-1} s^{-1}) at 7 T	$r_{1,paritcle}$ (mM^{-1} s^{-1}) at 7 T
Lip-DO3A@AuNP	14.6	34 675	4.0	9500
Lip-DTPA@AuNP	13.7	20 235	4.7	6942
DNA-Gd@AuNP	14.6[b]	8230[b]	5.8[b]	3270[b]

[a] "Ionic" r_1 refers to the contribution of each individual Gd(III) complex to proton relaxation, whereas "particle" describes the product of each particle's Gd(III) payload and ionic r_1.

[b] Reference 15.